



CHORUS

This is the accepted manuscript made available via CHORUS. The article has been published as:

First-principles prediction of switchable metallic ferroelectricity in multiferroic tunnel junctions

L. N. Jiang, W. Z. Chen, B. S. Yang, X.-G. Zhang, Yun-Peng Wang, and X. F. Han

Phys. Rev. B **99**, 224103 — Published 25 June 2019

DOI: [10.1103/PhysRevB.99.224103](https://doi.org/10.1103/PhysRevB.99.224103)

First-principles prediction of switchable metallic ferroelectricity in multiferroic tunnel junction

L. N. Jiang,^{1,2} W. Z. Chen,^{1,2} B. S. Yang,¹ X.-G. Zhang,^{3,*} Y.-P. Wang,⁴ and X. F. Han^{1,2,5,†}

¹*Beijing National Laboratory for Condensed Matter Physics,
Institute of Physics, University of Chinese Academy of Sciences,
Chinese Academy of Sciences, Beijing 100190, China*

²*Center of Materials Science and Optoelectronics Engineering,
University of Chinese Academy of Sciences, Beijing 100049, China*

³*Department of Physics and the Quantum Theory Project,
University of Florida - Gainesville, FL 32611, USA*

⁴*Department of Physics and Astronomy, Vanderbilt University, TN, 37235, USA*

⁵*Songshan Lake Materials Laboratory, Dongguan, Guangdong 523808, China*

(Dated: June 5, 2019)

Coexistence of metallicity and ferroelectricity has been a curiosity without a practical application, both because free electron screening due to metallicity prevents the polarization to be switched by an electric field, diminishing the value of ferroelectricity, and because metallicity is usually achieved by doping, which leads to disorder and is often detrimental to other electronic properties. Here, we predict via first-principles calculation a switchable metallic ferroelectric barrier in $(\text{Co}_2)_9\text{-TiO}_2\text{-(BaO-TiO}_2)_m\text{-CoO-Co}$ ($m = 4, 5, 6, 7, 8, 9$) multiferroic tunnel junction without doping. The metallic ferroelectricity is caused by an electrode proximity effect that is common to ionic ferroelectric materials and shifts the Fermi energy as a function of the termination layer at the interfaces. This effect is accentuated by the large polarization of CoO layer relatively to that of BTO, leading to a larger electrostatic potential drop on the interface containing CoO thus further pulling the conduction band bottom of the entire BTO region below the Fermi energy. Increasing the polarization of BTO relative to that of CoO, e.g., by applying strain, can remove the metallicity, allowing the polarization to be switched electrically. Switching between metallic and insulating states by controlling ferroelectric polarization leads to a large tunneling electroresistance.

INTRODUCTION

Ferroelectric (FE) materials are marked by a spontaneous polarization reversible by an external electric field [1]. This property can be combined with ferromagnetic (FM) electrodes to form multiferroic tunnel junctions (MFTJs) [2–4] to enable novel electronic devices designs. The interaction between the FE barrier and the FM electrodes in a MFTJ allows a multitude of possibilities for application [5, 6]. The conductance of a MFTJ depends on both the polarization switching of the FE barrier (tunneling electroresistance or TER) and relative direction of the magnetization arrangement of the two FM electrodes (tunneling magnetoresistance or TMR). TER and TMR are important performance parameters of MFTJs. A large TER effect usually arises from asymmetry in the FE barrier height [7–11] and width [7–9] under opposite polarization directions. In the extreme case, if the FE material is metallic under one polarization orientation and insulating the opposite polarization [12], the TER can be maximized.

In the past, ferroelectricity was considered to be unable to coexist with metallicity due to the screening effect of free electrons on the long-range Coulomb interaction, which was believed to be necessary for the FE phase [13]. However, counter examples have been known for a long time [14]. It is now recognized that a short-range part of the Coulomb interaction with the interaction range in the order of lattice constant is enough to cause ferro-

electricity [15], such as the polar metal LiOsO_3 [16–18]. When the free charge concentration in a conventional FE is low but above a metal-insulator critical concentration [15, 19], it cannot completely screen the 'short-range' Coulomb interaction, allowing the coexistence of ferroelectricity and metallicity. Ferroelectricity is lost only when the free charge concentration exceeds the FE critical concentration and both long-range and 'short-range' Coulomb interactions are screened [15]. This defines a narrow range of free electron concentration between the onset of metallicity and the disappearance of ferroelectricity. Experimental means to achieve metallic FE include doping [20], introducing vacancies [19] or electrostatic doping [21]. However, doping or introducing vacancies often lead to disorder. Even when metallic FE is achieved, its value for application may be limited due to the concern that its polarization might not be switchable electrically. Metallic charge can screen an applied electric field sufficiently to prevent the polarization from reversing. Ideally, metallic FE may be turned on and off by changing the pertinent bond lengths in the material, either by an applied strain along the polarization direction or by an applied electric field to switch the polarization.

In this work, we demonstrate from first-principles calculations that metallic FE BaTiO_3 (BTO) barrier in $(\text{Co}_2)_9\text{-TiO}_2\text{-(BaO-TiO}_2)_5\text{-CoO-Co}$ MFTJs terminated by two TiO_2 layers is switchable with strain. Due to the uncompensated charge layer at the BTO interface in this system, the BTO barrier has a tendency to acquire electrons. When two metal electrodes are very close to

BTO but not bonded with BTO, charge transfer still occurs from the electrodes to the barrier through tunneling. Such an electrode proximity effect moves the Fermi energy close to the barrier conduction band. When the polarization orientation points from the electrode with CoO layer to the other electrode (upward polarization), the relatively large (small) head-to-tail polarization of CoO (BTO) layer induces a larger electrostatic potential drop on the CoO layer than on BTO and causes the entire BTO barrier region to become metallic. Increasing the polarization of BTO by applying strain turns off the metallic FE. When the polarization is reversed (downward polarization), the Fermi level is also close to the conduction band due to the electrode proximity effect, but it remains in the band gap almost everywhere in the BTO barrier, maintaining an insulating state. This metallic-insulating BTO difference between two polarization configurations is shown to appear in $(\text{Co}_2)_9\text{-TiO}_2\text{-(BaO-TiO}_2)_m\text{-CoO-Co}$ system, where $m = 4, 5, 6, 7, 8, 9$, and leads to a sizable TER.

COMPUTATIONAL METHOD AND DETAILS

First-principles calculations are carried out using the Vienna ab-initio simulation package (VASP) [22] based on the density functional theory (DFT). Projector Augmented Wave (PAW) Pseudopotential [23, 24] and PBEsol generalized gradient approximation (GGA) exchange-correlation potential [25] are used. For clarity of presentation, we define the xyz directions in Fig. 1. The xy -plane lattice constant a is fixed at 3.906 Å. All calculations are spin-polarized. The plane wave cut-off energy is 500 eV. For structural relaxation, Gaussian smearing with $\sigma = 0.1$ eV and Gamma k-point mesh with $7 \times 7 \times 1$ are used. All atomic positions are relaxed along the z direction with a conjugate-gradient algorithm, until the residual force of each atom is less than 0.01 eV/Å. The self-consistent calculation at the final relaxed structure is carried out with the Gaussian smearing $\sigma = 0.05$ eV and k-point mesh of $16 \times 16 \times 1$. Structural relaxation is achieved by initially breaking the structural symmetry, giving different initial displacements of Ti and O atoms along the z direction. The total energy of $(\text{Co}_2)_9\text{-TiO}_2\text{-(BaO-TiO}_2)_5\text{-CoO-Co}$ MFTJs with upward polarization is about 0.143 eV lower than the downward polarization.

Additional calculations are performed to check whether the interfacial Co atoms have antiparallel moment alignment with respect to the Co electrodes. When the magnetization direction of the Co atoms in both CoO layer and the Co layer on the CoO/Co interface is antiparallel to the Co electrodes, the energy of the antiparallel configuration is about 0.537 (0.720) eV higher than the parallel configuration with upward (downward) polarization. Calculations are also performed to check whether the Co atoms in the CoO layer can form antiferromagnetic (AFM) states, by doubling the number

of atoms in the xy -plane. Calculations with fixed magnetic moments show that the energy of the AFM state is about 0.447 (0.535) eV higher than the FM state with upward (downward) polarization. We conclude that the Co atoms in both CoO layer and Co electrode have parallel magnetic moments.

RESULTS AND DISCUSSIONS

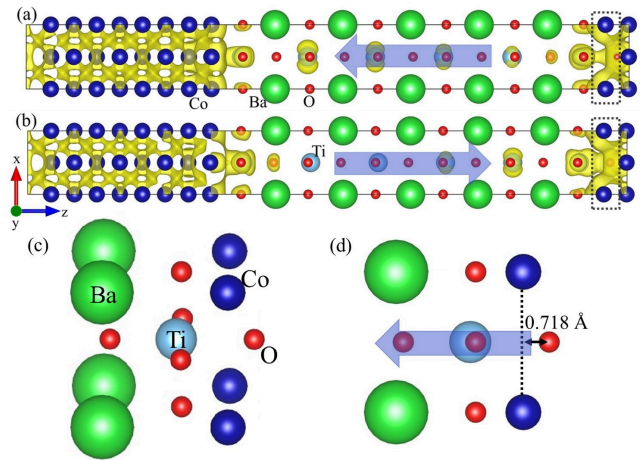


FIG. 1: The electronic charge density in the energy window from $E_F - 0.2$ eV to E_F in $(\text{Co}_2)_9\text{-TiO}_2\text{-(BaO-TiO}_2)_5\text{-CoO}$ structure for two opposite polarization. (a) upward polarization (b) downward polarization. Light blue arrows indicate the polarization direction. Dark blue, green, red and light blue represent the Co, Ba, O and Ti atoms. The CoO layer is marked by the black dotted line frame. (c) and (d) are the enlarged views of the interfacial BaO-TiO₂-CoO layers.

The structure of the junction and the charge density near the Fermi energy are shown in Fig. 1(a) and Fig. 1(b). Both sides of the BTO barrier terminate with the TiO₂ layer, similar to the structure of Fe/BTO MFTJs in reference [26]. The enlarged view of the interfacial BaO-TiO₂-CoO layers is shown in Fig. 1(c). The relative displacement of CoO layer indicated in Fig. 1(d) is 0.718 Å, which is much larger than that of Ti-O and Ba-O relative displacement. The yellow region in Fig. 1(a) and Fig. 1(b) shows the charge density for opposite polarization configurations calculated over an energy window from $E_F - 0.2$ eV to E_F . At the TiO₂-CoO interface, the charge density of Ti (in TiO₂ layer) and O (in CoO layer) atoms shows significant overlap in both panels, suggesting hybridization between the orbitals on the interfacial Ti and O atoms near the Fermi energy in both upward and downward polarization configurations. In the BTO region, the charge density of Ti atoms near the two interfaces is relatively high regardless of the upward or downward polarization configuration. For upward polarization, the high charge density extends from the interfaces to all BTO layers, suggesting the possibil-

ity of metallicity.

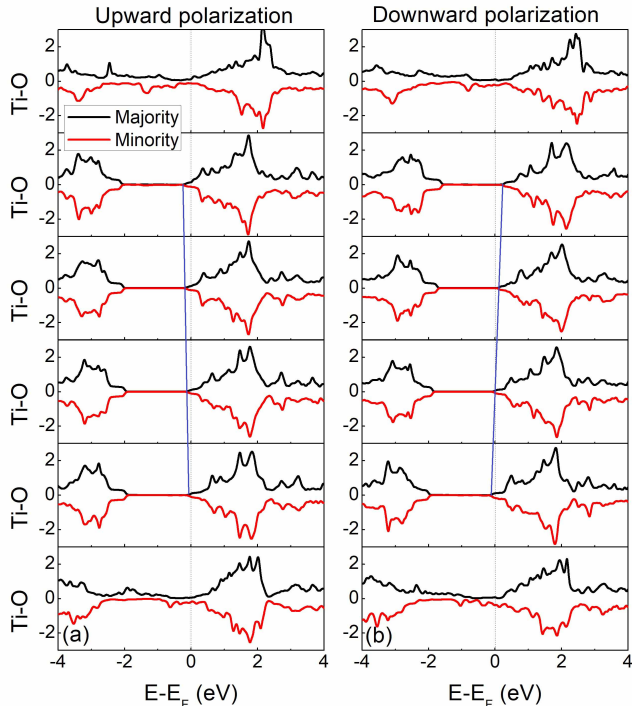


FIG. 2: Layer-resolved DOS of TiO_2 layers in $(\text{Co}_2)_9\text{-TiO}_2\text{-(BaO-TiO}_2)_5\text{-CoO}$ structure as a function of energy. From top to bottom, the DOS figures correspond from TiO_2 layer in $\text{Co}_2\text{-TiO}_2$ interface to TiO_2 layer in $\text{TiO}_2\text{-CoO}$ interface. (a) (b) are DOS for polarization pointing up and down, respectively. The blue solid line connects the CBM of each TiO_2 layer. Black (red) line is DOS of majority (minority).

The free-electron density can be estimated from the spin-polarized density of state (DOS) for each TiO_2 layer, which is plotted with smearing $\sigma = 0.05$ eV in Fig. 2 for majority-spin (black curves) and minority-spin (red curves). The DOS of the BaO layers is not plotted because their states are further away from the Fermi energy. The top (bottom) side corresponds to the $\text{Co}_2\text{-TiO}_2$ ($\text{TiO}_2\text{-CoO}$) interface. The conduction band minimum (CBM) in the FE barrier layers is marked by the blue solid line. The relative position of the Fermi level with the conduction band in upwardly polarized $(\text{Co}_2)_9\text{-TiO}_2\text{-(BaO-TiO}_2)_5\text{-CoO-Co}$ system implies a very high free electron concentration. For the upward polarization in Fig. 2(a), we integrated the DOS of each unit cell layer in the energy range from CBM to the Fermi energy to calculate the conduction band electrons concentration. Without considering the two interfacial TiO_2 layers, the free electron concentrations of different BTO unit cells are from 0.011 to 0.041 electrons per unit cell in upwardly polarized barrier, i.e., from 1.7×10^{20} to $6.4 \times 10^{20} \text{ cm}^{-3}$. This is above the metal-insulator transition critical concentration ($1.6 \times 10^{20} \text{ cm}^{-3}$ [27]), but not more than the critical concentration of ferroelectricity disappearance ($1.9 \times 10^{21} \text{ cm}^{-3}$ [15, 19]) in BTO barrier.

The estimate of the free electron concentration indi-

cates that the BTO layer under this condition is metallic. Yet such a metallicity may not be strong enough to kill ferroelectricity. The calculated Ti-O relative displacements along the z direction, measured from a reference plane of constant z , are 0.086 Å, 0.133 Å, 0.159 Å, 0.173 Å, 0.176 Å and 0.150 Å from the top to the bottom of the TiO_2 layers respectively, showing a non-centrosymmetric structure and ferroelectric nature. We conclude that the BTO barrier with upward polarization in this system is a metallic FE.

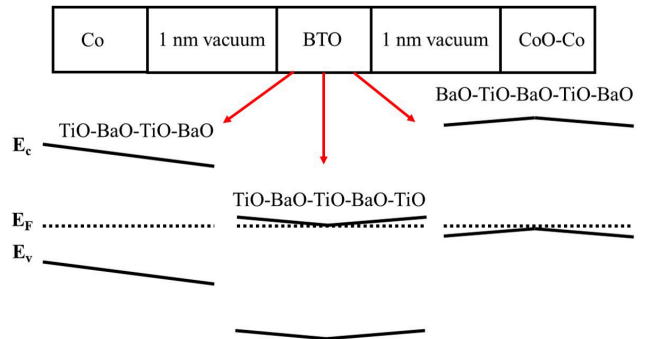


FIG. 3: Schematic diagram of band structures for BTO with different termination layers in $\text{Co}/1 \text{ nm vacuum}/\text{BTO}/1 \text{ nm vacuum}/\text{CoO}/\text{Co}$ system. The dotted line represents the Fermi level. The inclined conduction band E_c and valence band E_v are influenced by the polarization.

We first show that the Fermi energy is moved towards the conduction band bottom or valence band top in any ABO_3 ferroelectric barrier, where A and B are two metal elements with different valence charges, depending on the termination layers in contact with the metal electrodes. In Fig. 2 (a) and Fig. 2(b), the Fermi level is very close to the conduction band for both upward and downward polarization. The same phenomenon has been seen in many tunnel junctions with FE barriers [28–30]. The common occurrence of this phenomenon suggests a deeper reason for it. To identify its mechanism, we performed relaxation and self-consistent calculations with the BTO layer separated from the electrodes by additional vacuum layers. This removes the interface bonding effects and allows the pure electrode proximity effect to be isolated. The equilibrium self-consistent potential of $\text{Co}/1 \text{ nm vacuum}/\text{BTO}/1 \text{ nm vacuum}/\text{CoO}/\text{Co}$ with different termination layers for BTO are calculated. The Fermi energy relative to the band edges in the BTO layer is schematically shown in Fig. 3. For the structure of $\text{TiO-BaO-TiO-BaO-TiO}$, which has the same extra TiO layer as the $\text{TiO}_2\text{-(BaO-TiO}_2)_5$ structure in $(\text{Co}_2)_9\text{-TiO}_2\text{-(BaO-TiO}_2)_5\text{-CoO-Co}$ system, the Fermi level is very near the conduction band. For the structure of $\text{BaO-TiO-BaO-TiO-BaO}$, which has an extra BaO layer, the Fermi level is very near the valence band. For the structure of TiO-BaO-TiO-BaO where the two types of layers are equal in number, the Fermi level is near the middle of the band gap but a little closer to the valence band. Similar re-

sults are also obtained when we performed the calculations with the added vacuum layers but removed the CoO layer. These results indicate that the location of the Fermi level relative to the conduction band is mostly determined by an electrode proximity effect that is dependent on the termination layer.

The electrode proximity effect is distinct from the ‘pathological regime’ [31] caused by the well-known band-gap error of DFT calculation. First, the Fermi level remains in the middle of the band gap when the BTO termination layers are different on the two interfaces. This means that the DFT band-gap error itself does not cause any pathological charge transfer and metallicity. Second, when the BTO termination layers are the same on both interfaces (TiO-BaO-TiO-BaO-TiO or BaO-TiO-BaO-TiO-BaO), the Fermi level is moved to near the conduction band bottom or valence band top independently of the band gap size. Again, the DFT band-gap error has no effect.

The Bader charge analysis shows that the TiO-BaO-TiO-BaO-TiO barrier receives about 0.0133 electrons from the electrodes. This excess charge brings the Fermi level to near the conduction band. The same analysis for the BaO-TiO-BaO-TiO-BaO barrier shows that it loses about 0.0314 electrons, and for the TiO-BaO-TiO-BaO barrier shows that it loses about 0.0096 electrons. These charge transfers can account for most of the movements of the Fermi energy.

The effect discussed above pulls the Fermi level close to the conduction band in TiO₂-(BaO-TiO₂)₅ barrier, but it is not enough to pull the Fermi level into the conduction band in the entire barrier region. In the upwardly polarized configuration, the CBM of BTO barrier is below the Fermi level everywhere in the barrier region, as can be seen from Fig. 2(a). Interfacial bonding, as suggested by Fig. 1, which indicates strong hybridization between interfacial Ti and O atoms near the Fermi energy, is the last ingredient needed to explain this unusual phenomenon. The orbital-resolved DOS for Ti (in TiO₂ layer), O (in CoO layer) and Co (in CoO layer) atoms, as shown in Fig. 4(a)-(c), in TiO₂-CoO interface with polarization pointing up, shows clearly the hybridization between Ti-4s 3p_z 3d_{z²}, O-2s 2p_z and Co-4s orbitals. The hybridization between B-site 3d-orbital electrons and O 2p-orbital electrons is the main cause of ferroelectricity of ABO₃ perovskite structure, such as BaTiO₃ and PbTiO₃ [32]. If the A-site 4s-orbital electrons is also hybridized with the O 2p-orbital electrons, then the A-O hybridization will further enhance the polarization.

The metallicity of the interfacial CoO prevents an accurately calculation of the polarization contribution from this layer. However, the large relative displacement of 0.718 Å between Co and O atoms along the *z* direction in Fig. 1(d) indicates breaking of inversion symmetry in the CoO layer, and suggests a large polarization in the CoO region. We estimated the polarization contributions from individual layers for the upwardly polar-

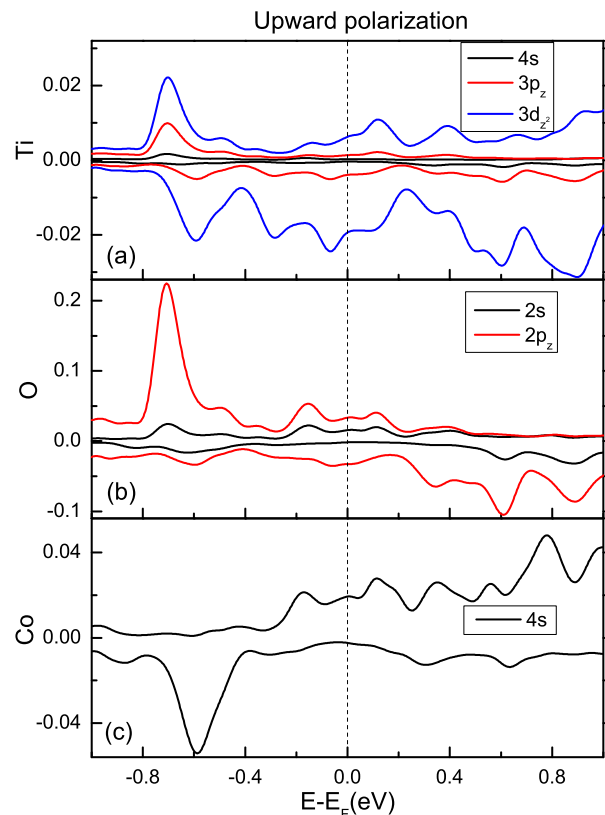


FIG. 4: Orbital-resolved DOS for Ti (in TiO₂ layer), O (in CoO layer) and Co (in CoO layer) atoms with upwardly polarized BTO barrier: (a) Ti-4s 3p_z 3d_{z²}, (b) O-2s 2p_z and (c) Co-4s. Upper and lower panels indicate majority-spin and minority-spin, respectively.

ized Co/BTO/CoO/Co using hybrid Wannier functions [33, 34], which is based on the Berry phase approach [35–37]. The calculated average polarization of metallic BTO is 22 μC/cm² per layer, which is smaller than that of the insulated BTO bulk 40 μC/cm², due to partial screening from the metallicity. In addition, the polarization of the TiO₂ layers (about 10 ~ 20 μC/cm² per layer) is much smaller than that of BaO layers (about 30 ~ 40 μC/cm² per layer). This is consistent with the calculated charge density, which shows that the conduction electrons mostly fall on the Ti atoms thus provide more screening in the TiO₂ layer. The calculated CoO polarization is 80 μC/cm² and is the largest of all layers.

Based on the roughly calculated polarization, we estimated the electrostatic potential drop of BTO and CoO. The relative dielectric constant ϵ/ϵ_0 of BTO (CoO) is about 100 ~ 300 [38, 39] (11) [40], the thickness of BTO (CoO) is 20 Å (2 Å), and the polarization of BTO (CoO) is 22 μC/cm² (80 μC/cm²). Simply based on $U = Ed = Pd/\epsilon$, the electrostatic potential drop on CoO can be estimated using $U = Pd/\epsilon \approx 1.643$ V. This is much larger than the potential drop on BTO as estimated from the polarizations (about 0.166 ~ 0.497 V depending on the value of the dielectric constant). The estimation for BTO

potential drop is confirmed by the first-principles calculation by comparing the DOS of the TiO₂ layers, which show the potential drop on BTO to be about 0.2 V.

Accordingly, the schematic diagram of the electrostatic energy across the tunnel junction is shown in Fig. 5. Here, $-e\Delta\varphi$, marked with red in the figure, is the energy difference between the Fermi energy and the CBM. This is calculated from the DOS of the TiO₂ layers. If $\Delta\varphi > 0$, the potential barrier profile in the entire BTO barrier region is below the Fermi level, leading to a metallic BTO for upward polarization. Relatively large CoO polarization P_2 and a small BTO polarization P_1 will lead to a larger electrostatic potential drop on the interface containing CoO than that on BTO, eventually giving rise to $\Delta\varphi > 0$. Therefore, by increasing P_1 or decreasing P_2 , $\Delta\varphi$ will be less than zero, and the metallicity will disappear.

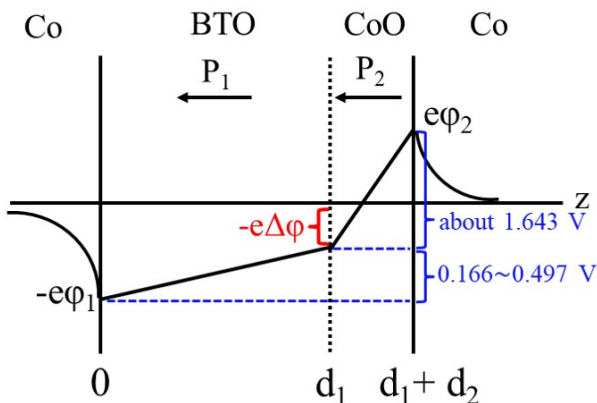


FIG. 5: Schematic diagram of electronic electrostatic energy for Co/BTO/CoO/Co with upward polarization. P_1 and P_2 with the same direction and different sizes are polarization of BTO and CoO layer, respectively. d_1 and d_2 are the thickness of BTO and CoO layer, respectively. The estimated electrostatic potential drops over the BTO and CoO regions are indicated with blue line and font.

To prove this by first-principles calculations in upwardly polarized Co/BTO/CoO/Co system, we increased the value of P_1 by applying strain along the polarization direction [41, 42] or reduced the value of P_2 by artificially reducing the relative displacement of Co and O along the z direction. When P_1 is increased by strain or P_2 is decreased by moving O atom to reduce the Co-O displacement, $\Delta\varphi$ is changed from positive to negative. The metallic BTO disappears under 2.7% strain or when the Co-O displacement decreases to less than 3/4 of the original distance, which is the Co-O distance along the z direction in the lowest energy Co/BTO/CoO/Co system. This allows the polarization to be switched electrically.

When the polarization is reversed, the metallic BTO is converted to an insulating BTO in this tunnel junction. As shown in Fig. 2(b), the Fermi level is also close to the conduction band due to the electrode proximity effect, but remains in the band gap almost everywhere in the

barrier. This metallic-insulating BTO difference between the two polarization configurations is predicted to appear in $(\text{Co}_2)_9\text{-TiO}_2\text{-(BaO-TiO}_2)_m\text{-CoO-Co}$ system, where $m = 4, 5, 6, 7, 8, 9$.

The conductance of a junction containing $(\text{Co}_2)_9\text{-TiO}_2\text{-(BaO-TiO}_2)_5\text{-CoO}$ with a $3.906 \text{ \AA} \times 3.906 \text{ \AA}$ cross section is calculated using Quantum Espresso. It is 0.2912×10^{-4} (0.4865×10^{-6}) e^2/h for upward (downward) polarization in the parallel configuration. TER is about 5885%. Although the calculated conductance has a large uncertainty due to its sensitivity to the barrier shape and height, and the latter is difficult to converge to a high degree of accuracy to yield a reliable conductance, the large TER is at least qualitatively correct.

Although the first-principles calculation has been performed on one type of multiferroic tunnel junctions, $(\text{Co}_2)_9\text{-TiO}_2\text{-(BaO-TiO}_2)_m\text{-CoO-Co}$, with $m = 4, 5, 6, 7, 8, 9$, the prediction of switchable metallic ferroelectricity through the mechanism of Fermi level shift due to charge transfer and relative large (small) polarization of CoO (BTO) via interfacial hybridization should be applicable to a general class of ferroelectric materials with uncompensated layer by layer charges. Whenever such a material is terminated at a metal/ferroelectric/metal interface with an uncompensated charge layer, the electrode proximity effect will move the Fermi energy close to the conduction band. Insertion of an appropriate interfacial layer with a much larger polarization than the ferroelectric barrier can cause the entire barrier region to become metallic ferroelectricity that is switchable.

ACKNOWLEDGMENTS

This work was supported by the National Key Research and Development Program of China [MOST, Grants No. 2017YFA0206200 and No. 2018YFB0407600], the National Natural Science Foundation of China [NSFC, Grants No.11434014, No.51620105004, and No.51831012], and partially supported by the Strategic Priority Research Program (B) [Grant No. XDB07030200], the International Partnership Program (Grant No.112111KYSB20170090), and the Key Research Program of Frontier Sciences (Grant No. QYZDJ-SSWSLH016) of the Chinese Academy of Sciences (CAS). XGZ is supported by National Science Foundation Grant No. ECCS-1508898. The atomic structure visualisation was produced with VESTA software [43]. The work was carried out at National Supercomputer Center in Tianjin, and the calculations were performed on TianHe-1 (A).

* Corresponding Author: xgz@ufl.edu

† Corresponding Author: xfhan@iphy.ac.cn

- [1] Y. Xu, *Ferroelectric Materials and Their Applications* (North-Holland, Amsterdam, 1991).
- [2] J. P. Velev, C. G. Duan, J. D. Burton, A. Smogunov, M. K. Niranjan, E. Tosatti, S. S. Jaswal, and E. Y. Tsymlal, *Nano Lett.* **9**, 427 (2009).
- [3] V. Garcia, M. Bibes, L. Bocher, S. Valencia, F. Kronast, A. Crassous, X. Moya, S. Enouz-Vedrenne, A. Gloter, D. Imhoff, C. Deranlot, N. D. Mathur, S. Fusil, K. Bouzehouane, A. Barthélémy, *Science* **327**, 1106 (2010).
- [4] D. Pantel, S. Goetze, D. Hesse, and M. Alexe, *Nat. Mater.* **11**, 289 (2012).
- [5] J. D. Burton and E.Y. Tsymlal, *Phys. Rev. Lett.* **106**, 157203 (2011).
- [6] Y. W. Yin, J. D. Burton, Y-M. Kim, A. Y. Borisevich, S. J. Pennycook, S. M. Yang, T. W. Noh, A. Gruverman, X. G. Li, E. Y. Tsymlal and Qi Li, *Nat. Mater.* **12**, 397 (2013).
- [7] M. Y. Zhuravlev, R. F. Sabirianov, S. S. Jaswal, and E. Y. Tsymlal, *Phys. Rev. Lett.* **94**, 246802 (2005)
- [8] Z. Wen, C. Li, D. Wu, A. Li, and N. B. Ming, *Nat. Mater.* **12**, 617 (2013).
- [9] X. Liu, J. D. Burton, and E. Y. Tsymlal, *Phys. Rev. Lett.* **116**, 197602 (2016).
- [10] R. Soni, A. Petraru, P. Meuffels, O. Vavra, M. Ziegler, S. K. Kim, D. S. Jeong, N. A. Pertsev, and H. Kohlstedt, *Nat. Commun.* **5**, 5414 (2014).
- [11] N. M. Caffrey, T. Archer, I. Rungger, and S. Sanvito, *Phys. Rev. Lett.* **109**, 226803 (2012).
- [12] V. S. Borisov, S. Ostanin, S. Achilles, J. Henk, and I. Mertig, *Phys. Rev. B* **92**, 075137 (2015).
- [13] W. Cochran, *Adv. Phys.* **9**, 387 (1960).
- [14] P. W. Anderson and E. I. Blount, *Phys. Rev. Lett.* **14**, 217 (1965).
- [15] Y. Wang, X. Liu, J. D. Burton, S. S. Jaswal and E. Y. Tsymlal, *Phys. Rev. Lett.* **109**, 247601 (2012).
- [16] Y. Shi, Y. Guo, X. Wang, A. J. Princep, D. Khalyavin, P. Manuel, Y. Michiue, A. Sato, K. Tsuda, S. Yu, M. Arai, Y. Shirako, M. Akaogi, N. Wang, K. Yamaura, and A. T. Boothroyd, *Nat. Mater.* **12**, 1024 (2013).
- [17] H. M. Liu, Y. P. Du, Y. L. Xie, J.-M. Liu, C.-G. Duan, and X. Wan, *Phys. Rev. B* **91**, 064104 (2015).
- [18] H. J. Xiang, *Phys. Rev. B* **90**, 094108 (2014).
- [19] T. Kolodiazny, M. Tachibana, H. Kawaji, J. Hwang and E. Takayama-Muromachi, *Phys. Rev. Lett.* **104**, 147602 (2010).
- [20] X. He and K.-j. Jin, *Phys. Rev. B* **94**, 224107 (2016).
- [21] S. Raghavan, J. Y. Zhang, O. F. Shoron, and S. Stemmer, *Phys. Rev. Lett.* **117**, 037602 (2016).
- [22] G. Kresse and J. Furthmüller, *Phys. Rev. B* **54**, 11169 (1996).
- [23] P. E. Blöchl, *Phys. Rev. B* **50**, 17953 (1994).
- [24] G. Kresse and D. Joubert, *Phys. Rev. B* **59**, 1758 (1999).
- [25] J. P. Perdew, A. Ruzsinszky, G. I. Csonka, O. A. Vydrov, G. E. Scuseria, L. A. Constantin, X. Zhou, and K. Burke, *Phys. Rev. Lett.* **100**, 136406 (2008).
- [26] B. Yin and S. Qu, *Phys. Rev. B* **89**, 014106 (2014).
- [27] T. Kolodiazny, *Phys. Rev. B* **78**, 045107 (2008).
- [28] J. P. Velev, C.-G. Duan, K. D. Belashchenko, S. S. Jaswal, and E. Y. Tsymlal, *Phys. Rev. Lett.* **98**, 137201 (2007).
- [29] C.-G. Duan, S. S. Jaswal, and E. Y. Tsymlal, *Phys. Rev. Lett.* **97**, 047201 (2006).
- [30] D. Cao, M.-Q. Cai, W. Y. Hu and C.-M. Xu, *J. Appl. Phys.* **109**, 114107 (2011).
- [31] M. Stengel, P. Aguado-Puente, N. A. Spaldin, and J. Junquera, *Phys. Rev. B* **83**, 235112 (2011).
- [32] R. E. Cohen, *Nature (London)* **358**, 136 (1992).
- [33] X. Wu, O. Diéguez, K. M. Rabe, and D. Vanderbilt, *Phys. Rev. Lett.* **97**, 107602 (2006).
- [34] Y.-P. Wang and H.-P. Cheng, *Phys. Rev. B* **91**, 245307 (2015).
- [35] R. D. King-Smith and D. Vanderbilt, *Phys. Rev. B* **47**, 1651 (1993).
- [36] D. Puggioni, G. Giovannetti, M. Capone, and J. M. Rondinelli, *Phys. Rev. Lett.* **115**, 087202 (2015).
- [37] C. He, Z. Ma, B.-Z. Sun, Q. Li, and K. Wu, *Comput. Mater. Sci.* **105**, 11 (2015).
- [38] L. Pintilie, I. Vrejoiu, D. Hesse, G. Le Rhun, and M. Alexe, *Phys. Rev. B* **75**, 224113 (2007).
- [39] B. Lee and J. Zhang, *Thin Solid Films* **388**, 107 (2001).
- [40] K. V. Rao and A. Smakula, *J. Appl. Phys.* **36**, 2031 (1965).
- [41] H. N. Lee, H. M. Christen, M. F. Chisholm, C. M. Rouleau, and D. H. Lowndes, *Nature (London)* **433**, 395 (2005).
- [42] D. Odkhuu and N. Kioussis, *Phys. Rev. B* **97**, 094404 (2018).
- [43] K. Momma and F. Izumi, *J. Appl. Crystallogr.* **44**, 1272 (2011).